Multiphoton process investigation in silica by UV femtosecond laser

Vincenzo de Michele, Emmanuel Marin, Aziz Boukenter, Marco Cannas, Sylvain Girard, Youcef Ouerdane

Version of Record: https://www.sciencedirect.com/science/article/pii/S0022309321007456
Manuscript_6755d513fe5fbd47e8f3df1dce403b9b

Journal of Non-Crystalline Solids – For review only

Multiphoton Process Investigation in Silica by UV Femtosecond Laser

Vincenzo De Michele[1,2,*], Emmanuel Marin[1], Aziz Boukenter[1], Marco Cannas[2], Sylvain Girard[1], and Youcef Ouerdane[1]

1. Université de Saint-Etienne, Laboratoire Hubert Curien, UMR-CNRS 5516, 18 rue Prof. B. Lauras, F-42000 Saint-Etienne, France

2. Department of Physics and Chemistry "Emilio Segrè", University of Palermo, Via Archirafi 36, 90123 Palermo, Italy

* Corresponding author: vincenzo.demichele@univ-st-etienne.fr ; +33 7 67 26 59 12

Co-authors: emmanuel.marin@univ-st-etienne.fr ; aziz.boukenter@univ-st-etienne.fr ; marco. cannas@unipa.it ; sylvain.girard@univ-st-etienne.fr ; ouerdane@univ-st-etienne.fr

Abstract – We investigated the interaction processes between high intensity femtosecond ultraviolet laser pulses and amorphous silica, leading to permanent refractive-index changes that are at the basis of advanced manufacturing for photonics devices. The experiment, carried out as a function of the laser power, improves our understanding on the strong-field ionization process by the monitoring of the 1.9 eV and 2.65 eV emissions, related to nonbridging oxygen hole centers and self-trapped exciton, respectively, induced in the exposed glass region. Our results clearly proved that the UV laser light band-to-band absorption is allowed in the multiphoton ionization limit, whose consecutive relaxation leads to the generation of these photoluminescence (PL) signatures. Furthermore, we coupled the online PL investigation with post mortem analysis of the irradiated volume through phase contrast microscopy, Raman and steady state PL, providing a complete view of the silica-femtosecond laser interaction.

Keywords – Silica, Point defects, Strong-field ionization, Femtosecond laser, Photoluminescence

Highlights

- Non-linear deposition of the light investigated by online photoluminescence induced by UV femtosecond laser exposition.
- Clarification of the strong-field ionization limit (multiphoton regime) which leads to the generation of point defects under femtosecond laser irradiation.
- Understanding of the OH content impact on the silica-femtosecond laser interaction monitoring the optical signatures of the PL-active induced defects.
- Evidence of the importance of online investigation to better understand the fs laser-silica interaction processes compared to the post mortem one.

Multiphoton Process Investigation in Silica by UV Femtosecond Laser

Introduction

The extremely short pulse temporal width of sub-picosecond lasers has pushed forward the technology of integrated photonics in wide band-gap materials, allowing to achieve new optical properties [1–4]. A relevant example consists in the inscription of waveguides or Bragg gratings of controlled period by focused femtosecond (fs) laser pulses, able to induce permanent refractive-index change (RIC) in the material [5–8]. Indeed, focusing ultrashort high-intensity laser pulses into bulk dielectrics, it is possible to excite electrons in the conduction band [9–11] by laser-induced strong-field ionization (SFI), according to the multiphoton ionization (MPI) and/or strong ionization field (tunneling ionization) regimes of interaction. MPI consists in the simultaneous absorption of several photons, induced at the typical intensity reached by femtosecond pulsed lasers. For this phenomenon, the rate of photons' absorption W_{MPI} is driven by the following relation:

$$W_{MPI} \propto I^{N}. \quad (1)$$

Where I is the laser intensity and N the number of photons necessary to realize the band-to-band transition [10,12,13].

The tunneling photoionization regime is dominant when the electric field induced by the laser pulses is high enough to distort the potential wall that maintains the electrons bounded to the nuclei, allowing a transition from the valence to the conduction band [14]. With such nonlinear ionization processes, the induced damage, driven by the density and the temperature distribution of the generated plasma in the focal region, could be controlled with a ~µm to ~nm precision scale [7]. The development of highly localized structural modifications on transparent material leads to potential applications in telecommunications, optical sensing and optical signal processing domains [6,8].

Despite the importance of the nonlinear light absorption on high-intensity laser-based technology, it also plays a crucial role in solid-state physics from several points of view. Nonlinear absorption limits the transmission properties of transparent materials, leading to color centers' generation as well as important permanent structural modifications, such as densification and/or hollow voids and shock waves in the focal region [2–4]. SFI is particularly efficient in generating a uniform concentration of careers along the illuminated

volume, unlike linear absorption, which is generally attenuated at the sample surface [10]. Moreover, SFI could be used to investigate the intrinsic processes leading to the non-linear absorption of the light, providing unique information on the laser-material interactions.

In this framework amorphous silica (a-SiO_2) is a reference among transparent materials, particularly suitable for applications deriving from the interaction with ultrashort laser pulses. Its electronic structure is mainly determined by the fundamental unit SiO_4 tetrahedron and is, therefore, quite similar to that of crystalline α-quartz; experimentally, this results in a comparable bandgap energy of ~9 eV [15]. Previous studies have demonstrated that the nonlinear deposition of laser energy into silica follows two types of interaction regimes, depending on the experimental conditions [2,16,17]: Type I, characterized by positive and isotropic RIC, and Type II, which corresponds to a negative RIC, coupled with the appearance of birefringent phenomena. The spectroscopic fingerprint of Type I [2,17–19] is the typical Non-Bridging-Oxygen-Hole-Center (NBOHC) PL band peaking at 1.9 eV (650 nm), while the Type II [2,17] is characterized by a PL band at ~2.3 eV (540 nm), whose origin is still debated.

In the present work we investigate the PL acquired under 3.6 eV (343 nm) fs laser irradiation (online PL) of the induced defects in silica. The experiment is carried out as a function of the laser pulse power on two silica samples differing by their hydroxyls groups (OH) contents, highlighting the regime governing the strong field response of the samples. Indeed through fs irradiation we compare the SFI, in the multiphoton limit, influence on the matrix (intrinsic process) with the one involving the OH groups (extrinsic process) [20], monitoring the optical signature of the induced PL-active point defects. Furthermore, the post mortem characterization of the laser damaged area clarifies how online measurements provides more in-depth information on the light-matter interaction.

Experimental description

The tested specimens are two different highly-transparent polished silica glasses (dimensions~20×10×4 mm^3) with different OH contents: a synthetic dry silica, with [OH]<10 ppm (Suprasil 300), and a synthetic wet silica with [OH]~1000 ppm (Corning 7980).

The online PL experiment is performed with a homemade setup, reported in Figure 1, probing the induced photoluminescence as a function of the pulse peak power (between 0.15 MW and 0.40 MW). The ~3.6 eV (343 nm) irradiation beam is provided by the harmonic generator

HIRO (Light Conversion), producing the third harmonic from the ~1.2 eV (1030 nm) fundamental signal, generated by a PHAROS (Light Conversion) femtosecond laser. The temporal pulse width is about ~200 fs and the whole experiment is performed with a repetition rate of 1 kHz. The beam power is controlled by a half-wave plate (HWP) followed by a polarizer (P) at the output of the HIRO module. Moreover, to ensure that the irradiated sample's surface is perpendicular to the beam direction, a LED source (collinear with the laser direction) is paired with a CMOS camera (from Thorlabs) in back reflection configuration, to align and focalized the probe signal onto the sample's surface (not present in Figure 1). The experiment is performed in transversal geometry. The femtosecond pulses are focalized into the specimen bulk through a UV objective with a numerical aperture NA=0.5 and the induced isotropic PL is collected by a telescope used to focalize the signal directly into the spectrometer (Hamamatsu), working in the [3.88 eV (320 nm) - 1.16 eV (1070 nm)] spectral range. During the exposure, the detector integration time is set to 100 ms, measuring every spectra as an average of 100 pulses, irradiating for a total ~10^4 pulses at each fixed power. Since the collected light mainly arises from the plasma emission in the focal spot, during the experiment the detection is focused above the focal point. For each power, the sample is shifted of 50 µm using a motorized translation stage (from Thorlabs), to avoid the induced damage overlap on the sample.

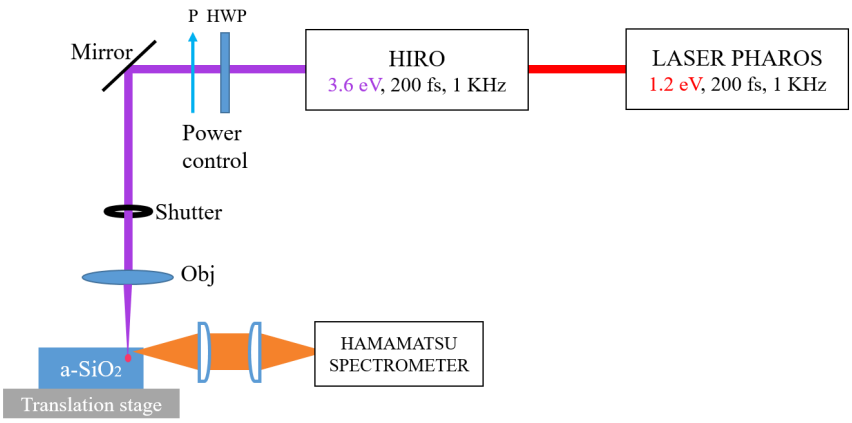

Figure 1. Experimental setup for online PL measurements upon UV fs laser exposure.

To characterize the induced damage, we also performed a post mortem analysis, probing the induced RIC distribution and studying the permanent structural modification such as the presence of induced PL-active stable defects or possible network modifications. The former was probed in the damaged region by phase contrast microscopy (ZEISS AXIO microscopy) in transmission configuration. The latter through steady state PL and Raman measurements employing an integrated confocal micro-spectrometer ARAMIS (Horiba Jobin-Yvon) in

backscattering configuration, equipped with a He-Cd CW probe laser line at ~3.8 eV (325 nm). The micro-spectrometer parameters are set in order to obtain a ~5 μm spatial resolution in the XY plane thanks to a confocal pinhole of 70 μm diameter. A spectral resolution of ~5 cm^{-1} was achieved with 2400 lines/mm grating for the Raman measurements.

Results and Discussion

Synthetic dry silica

Figure 2 shows the PL spectrum acquired after ~10^4 pulses, irradiated at a pulse peak power of ~0.40 MW, while the inset reports the zoom between 2.0 eV and 3.1 eV. Two spectral features are clearly distinguishable: an asymmetric band peaked at ~1.9 eV, associated with the well-known photoluminescence of the NBOHC [20,21]; a Gaussian shaped band centered at

~2.65 eV with a FWHM~0.4 eV. Regarding the last band, at least two PL-active defects are known to emit in this spectra region: the self-trapped excitons (STX), that are observed both in amorphous and crystalline SiO_2 [22–24], and the oxygen deficiency centers (ODC (II)) [25–27].

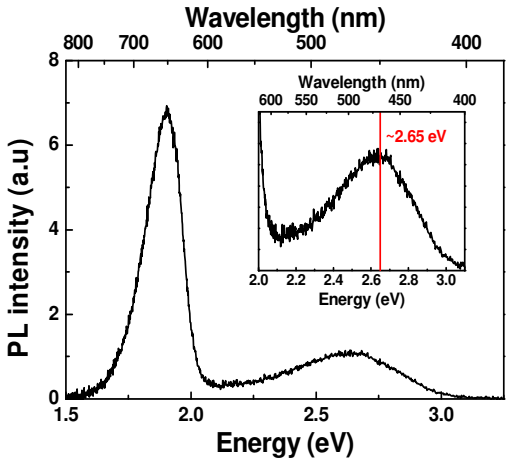

Figure 2. Suprasil 300 PL spectrum acquired with 3.6 eV femtosecond laser pulses, after ~10^4 pulses at pulse peak power of ~0.40MW. The inset shows the zoom of the spectral region between 2.0 eV and 3.1 eV.

To deeply study the dependence of the 1.9 eV and 2.65 eV bands as a function of the pulse number (equivalent to the irradiation dose), Figure 3 reports the spectra acquired after different numbers of accumulated laser pulses (N_p). The inset shows the evolution of the normalized PL intensity (I_{PL}) recorded at 1.9 eV and 2.65 eV, on increasing N_p. These results suggest the same precursor site for the two bands that scale equally as a function of N_p. In particular, it is possible to distinguish two different generation regimes: i) transient linear

regime I_{PL} proportional to N_p, up to ~800 pulses; ii) sublinear dependence, after ~800 pulses, revealing an intrinsic generation process, that is described by equation 2 [20]:

$$I_{PL} \propto (N_p)^n \qquad (2)$$

where the n parameter range is $0 < n < 1$. The best fit value is found to be n=0.33. The same trend is observed in the other measurements done varying the laser power.

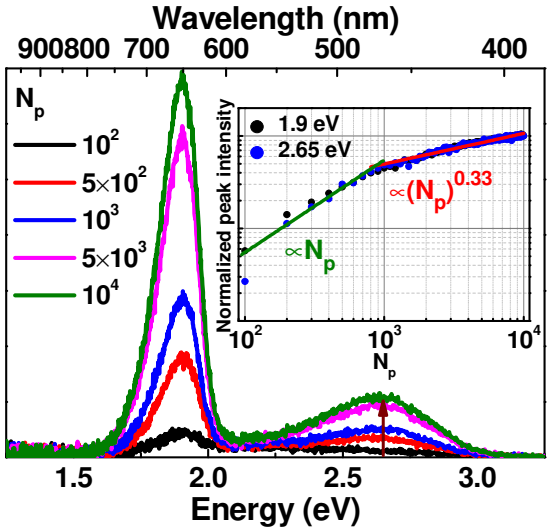

Figure 3. Suprasil 300 PL spectra at different accumulated numbers of laser pulses: 10^2 pulses (black), 5×10^2 (red), 10^3 (blue), 5×10^3 (magenta) and in green after 10^4 pulses. The inset reports the evolution of the peak intensity as a function of the number of the pulses at pulse peak power of ~0.40MW, normalized with respect to the PL value at 10^4 pulses, at 1.9 eV and 2.65 eV, in black and blue circles respectively. The red line represents the best fit curve according to equation 2.

The observed kinetics indicate that the generation mechanism of the NBOHCs is a consequence of $Si-O-Si$ breaking bond [20,28–30]:

$$\equiv Si - O - Si \equiv \xrightarrow{\hbar\omega} \equiv Si - O \cdot + \cdot Si \equiv \qquad (3)$$

with simultaneous generation of E´ center, that is a very well characterized paramagnetic defect in silica, which absorbs in UV at 5.8 eV without any emitting PL band [27, 31].

It is important to stress that the Suprasil 300 sample, in linear absorption conditions, is transparent to the incoming photons, then, only nonlinear processes are expected exciting at 3.6 eV (343 nm). By monitoring the dependence of the PL-active induced defects, it is possible to identify the nonlinear absorption regime of the deposited laser energy. In fact, considering the PL-active induced defects generated by MPI, as a consequence of the

equation (1), the PL intensity is also proportional to the N_{th} power of the incident light intensity I [10,12,13,32]:

$$I_{PL} \propto I^{N}, \qquad (4)$$

where N is the number of photons necessary to realize the band-to-band transition. Therefore, it is possible to determine the order of nonlinear light absorption process studying the PL intensity as a function of the pulse peak power. Figure 4 reports the PL dependence at both 1.9 eV and 2.65 eV as a function of the laser power acquired after 10^4 pulses (sub-linear regime) and after 500 pulses (linear regime) respectively. In the figure, the two data sets are scaled for a direct and easy trend comparison. In both cases, a super linear dependence with N=3±0.2 (red straight lines in the figure) is evident, supporting a pure-multiphoton absorption regime. Particularly, the absorption of three 3.6 eV photons agrees with a band-to-band transition around ~10.8 eV, which is close to the first excitonic absorption peak at 10.4 eV [33,34], suggesting the generation and the self-trapping of an exciton. This exciton leads to the deformation and then the breaking of the $Si-O-Si$ bond that is characterized by the emission of photons at 2.65 eV coupled with the NBOHC and E´ centers generation [35], explaining the origin of such PL band, according to equation 3. The inset in figure 4(a) shows the normalized spectra after 10^4 pulses, acquired at the highest and lowest investigated laser powers respectively: the comparison provides evidence that the induced PL maintains the same shape, regardless of the laser power. It is important to remark that at laser powers lower than 0.15 MW no PL is observed within the detection limits.

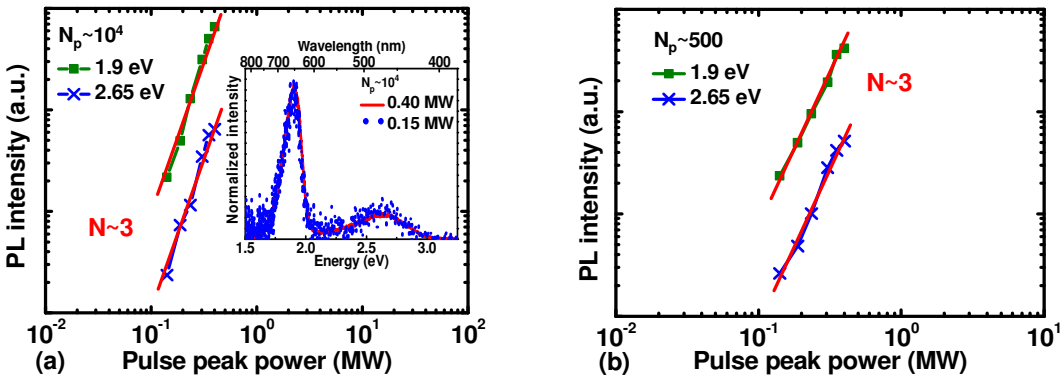

Figure 4. Suprasil 300 PL intensity evolution at both 1.9 eV (green) and 2.65 eV (blue) as function of the pulse peak power after 10^4 and 500 pulses respectively (a) and (b). The red lines represent the best fit curves according to equation 4. The two data sets referred to the 1.9 eV and 2.65 eV PL bands are scaled for a direct and easy trend comparison. The inset represents the normalized PL spectra at the highest and lowest investigated laser powers.

Synthetic wet silica

An analogous investigation was performed on the Synthetic wet silica sample (Corning 7980), characterized by a higher OH content (~1000 ppm) compared to the Suprasil 300. The online PL spectra at ~0.40 MW and different pulse numbers is reported in Figure 5 (a), while Figure 5 (b) presents the normalized kinetics of the peaks intensities at 1.9 eV and 2.65 eV. The observed spectral features are similar to those already encountered in the Suprasil 300, but with different relative amplitudes: the NBOHC related PL band centered at 1.9 eV, and the 2.65 eV peaked band, already attributed to the STX. In Figure 5 (b), the 2.65 eV kinetic could be described by an intrinsic process from the beginning of the irradiation, finding n=0.33 according to equation 2, while the 1.9 eV PL shows a totally different behavior. In the present sample, this kinetic reaches a maximum value around 500 pulses, to decrease down after to the value measured after 10^4 pulses. Analogous trends are observed at lower laser powers. The explanation of this behavior is attributed to the high OH content, which introduces an extrinsic process described by [20]:

$$\equiv \mathrm{Si} - \mathrm{OH} \xrightarrow{\hbar\omega} \equiv \mathrm{Si} - \mathrm{O} \cdot + \mathrm{H}, \qquad (5)$$

leading to the NBOHC generation through the breaking of OH bonds. It is possible to argue that the fast growth is due to the OH conversion into NBOHC, and once these precursor sites are exhausted, notwithstanding the intrinsic process, the number of bleached NBOHC is dominant [35]. The nature of the observed bleaching could be linked to unstable defects induced at RT or directly by the incident laser pulses. Therefore, at fixed laser fluence, we observed two different pathways for the NBOHC's generation: an extrinsic dominant process, described by equation 5 and driven by the high OH content in the sample, and an intrinsic one, consequent to the STX relaxation, as described by equation 3.

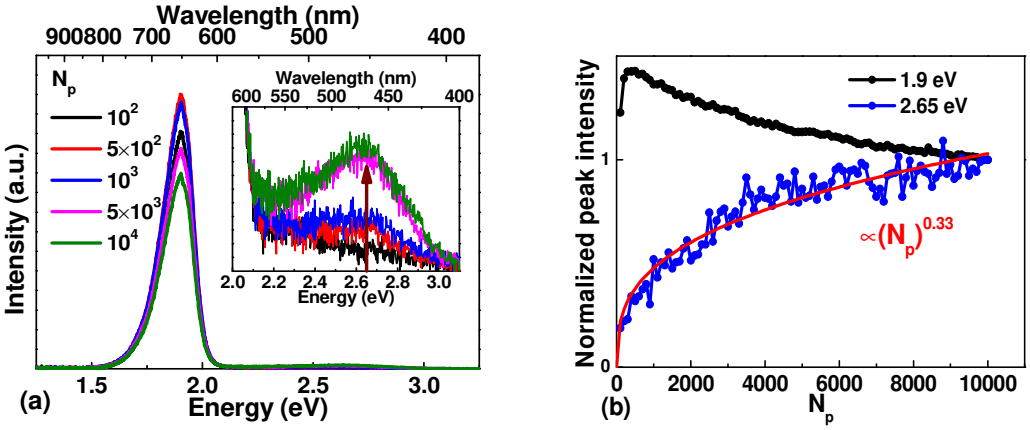

Figure 5. (a) Corning 7980 sample PL spectra at different accumulated pulses: 10^2 pulses (black), 5×10^2 (red), 10^3 (blue), 5×10^3 (magenta) and in green after 10^4 pulses, with a pulse power of ~0.40 MW. The inset zooms the spectral region between 2.0 eV and 3.1 eV. (b) Kinetics of the peak intensity measured at ~0.40MW, normalized to the PL value at 10^4 pulses, for at the 1.9 eV (black) and 2.65 eV (blue) bands respectively. The red line represents the best curve fit according to equation 2.

Figure 6 shows the PL intensities, measured at both 1.9 eV and 2.65 eV as a function of the laser pulse peak power, after 10^4 pulses (Figure 6 (a)), at the end of the irradiation, and at 500 pulses (Figure 6 (b)), associated to the maximum PL intensity at 1.9 eV in Figure 5 (within the extrinsic process generation). In the figure, the two data sets are scaled for a direct and easy trend comparison. In Figure 6 (a) the two contributions follow the same power law, suggesting newly the SFI process in the multiphoton regime requiring ~3 photons for the same band-to-band transition already reported for the Suprasil 300 glass.

A different behavior is observed in Figure 6 (b) after 500 pulses: the intrinsic process represented by the normalized PL at 2.65 eV is still characterized by N=3±0.2, according to equation 4, while the 1.9 eV PL band shows a slightly different kinetic with N=2.6±0.2. Albeit in the present case the PL dependence on the laser pulse peak power suggests a multiphoton absorption, it is near to the energy value required for the OH breaking bond [20,30], which drives the extrinsic process.

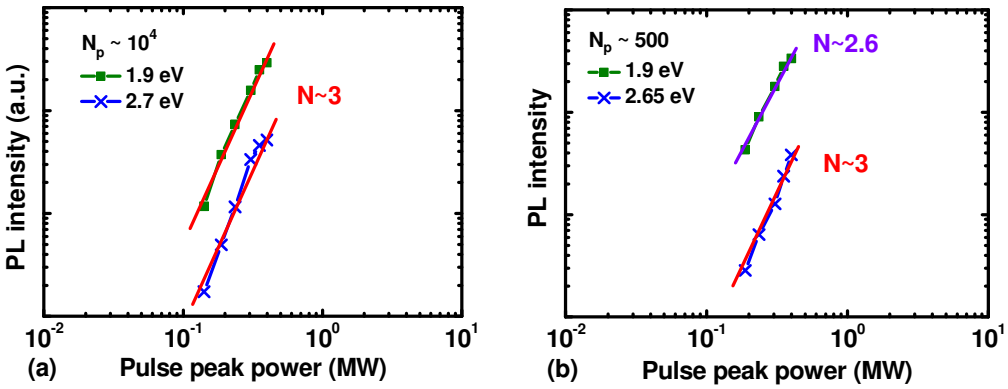

Figure 6. PL Corning 7980 intensity evolution at 1.9 eV (green) and 2.65 eV (blue) as function of the pulse peak power after 10^4 and 500 pulses respectively (a) and (b). The red and violet lines represent the best fit curves according to equation 4. In both figures, the two data sets are arbitrarily scaled for viewing purposes.

Post mortem Characterization

Figure 7 depicts the PCM image, as a function of the laser power, over the entire UV fs laser exposed area in the Suprasil 300 sample. In the figure, darker and brighter zones originate from the increase and decrease of the refractive index, respectively, compared to the surrounding medium. The elongated damage along the laser direction and its width depend on the pulse peak power. Being the darker color a fingerprint of positive Δn, uniform smooth isotropic positive refractive index changes are observed at low pulse powers (0.15 MW ÷ 0.25 MW), indicating a gentle material response as a consequence of a soft laser-induced excitation (trace inside the blue delimited zone in Figure 7). At higher laser powers, the damaged area presents a more complex panorama: the intense energy concentration was able to drive the matrix into strong matter reaction, resulting in non-uniform damaged area in the focal spot (trace inside the red delimited zone in Figure 7). In particular, for pulse peak powers higher than 0.25 MW, the laser traces are reported in brighter and darker colors, with respect to the background (surrounding glass matrix), suggesting a transition from the Type I to Type II interaction regimes [2,17].

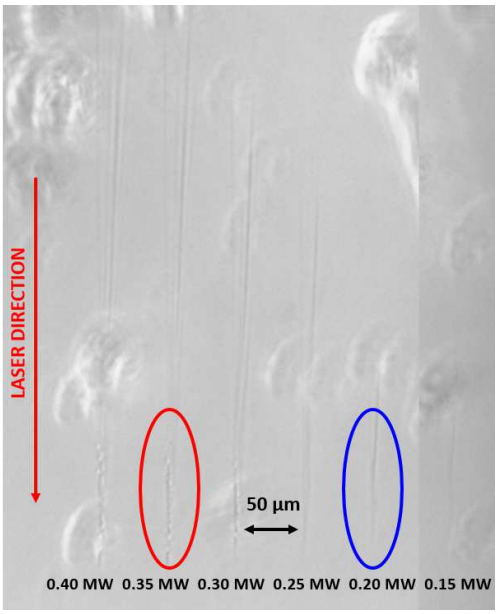

Figure 7. PCM image of the induced damages under 3.6 eV femtosecond pulses at different pulse peak powers for the Suprasil 300 sample. The red arrow indicates the laser direction propagation. The blue and red zones focus the reader on the morphological properties of the uniform smooth isotropic positive refractive index change trace and the uneven area damaged at high power, respectively.

An analogous discussion is valid for the Corning 7980 sample. It is important to note that the post mortem analysis did not reveal any difference between the two materials, thus highlighting the crucial importance of PL online measurements to better understand the laser-induced effects on silica samples with different OH content.

Similarly, Figure 8 is representative of the steady state PL and Raman post mortem characterizations of the two samples: both types of spectra are taken in the laser focal point, whose location was individuated by the higher PL signal originating from the laser induced defects. The PL acquisitions show the typical features of the Type I (at low pulse powers) and Type II (at high pulse powers) interaction regimes upon ~3.8 eV (325 nm) excitation, indicating ~0.30 MW as the Type I/II power threshold. Notwithstanding the smooth positive refractive index change observed at lower powers, no densification is highlighted by Raman spectra of the damaged area (Figure 8 (b)). This could be due basically to a very smooth densification, below the experimental sensitivity, or that the positive refractive index change depends, through the Kramers-Kronig relation, on the induced absorption defects.

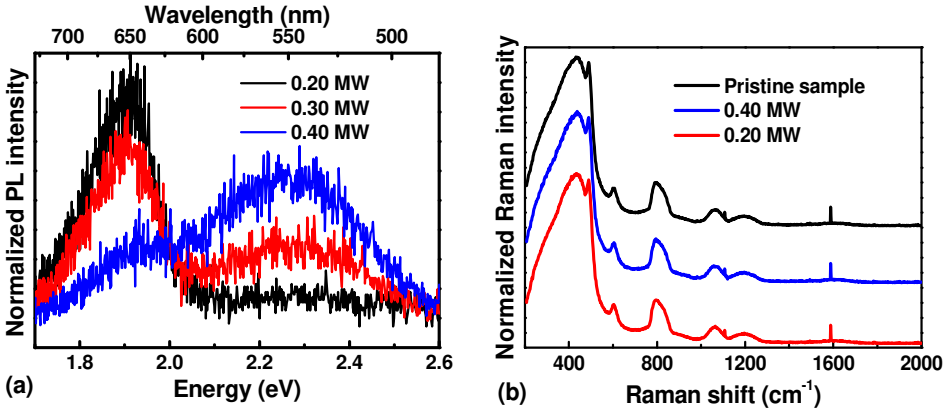

Figure 8. (a) Suprasil 300 Post mortem PL spectra, scaled for the area, of the laser induced traces at different powers: 0.20 MW (black), 0.30 MW (red) and 0.40 MW (blue). (b) Comparison between the Raman spectra, measured in the Suprasil 300 sample, acquired in the pristine sample (black line), 0.40 MW (blue line) and at 0.20 MW (red line).

Conclusions

In the present work we have studied the nonlinear absorption of high intensity femtosecond ultraviolet pulses in amorphous silica monitoring the induced PL as a function of the laser power in samples having different OH contents. The observed spectral features have very close similarities in the two investigated samples: the NBOHC related PL band peaked at 1.9 eV and the STX emission band at 2.65 eV. The samples' chemical composition plays an important role in the NBOHC response, manifesting two different scenario: i) intrinsic generation process, observed in the sample with low OH content, caused by the STX relaxation as consequence of a band-to-band SFI process in the multiphoton ionization regime; ii) extrinsic process, observed in samples with relevant OH concentration, in which the NBOHC generation is driven by the breaking of OH bonds followed by a transition to an intrinsic behavior at higher fluencies. In particular we observed a non-monotonous evolution of the NBOHC band, highlighting a transition from an extrinsic generation process to an intrinsic one.

The MPI regime is revealed by the super-linear dependence of the PL intensity as a function of the laser power, suggesting that the NBOHC generation is basically due to the STX relaxation, coupled with the 3-photons absorption, which is in accordance with the first excitonic absorption peak. Different behaviors between the two samples are observed at low total accumulated doses: if the total PL intensity is still a third multiphoton order absorption process in the Suprasil 300, for the Corning 7980, at low doses the NBOHC's multiphoton

absorption order is characterized by N~2.6, which is near to the OH broken bond energy, strongly supporting the presence of the extrinsic process.

The post mortem analysis of the exposed regions reveals the Type I/Type II transition in the investigated power range, confirmed both from the PCM and PL measurements, while no glass densification is observed. No difference between samples was individuated by the post-mortem analysis, highlighting the importance of the online investigation to better understand the 'fs laser - amorphous silica' interaction processes.

References

[1] D. Strickland and G. Mourou, "Compression of amplified chirped optical pulses," *Optic Commun.* 56, pp. 219-221 (1985).

[2] K. Mishchik, C. D'Amico, P. K. Velpula, C. Mauclair, A. Boukenter, Y. Ouerdane, and R. Stoian, "Ultrafast laser induced electronic and structural modifications in bulk fused silica," *J. Appl. Phys.* 114, 133502 (2013).

[3] S. S. Mao, F. Quéré, S. Guizard, X. Mao, R. E. Russo, G. Petite, and P. Martin, "Dynamics of femtosecond laser interactions with dielectrics," *Appl. Phys. A* 79, pp. 1695-1709 (2004).

[4] T. E. Itina, O. Utéza, N. Sanner, M. Sentis, "Interaction of femtosecond laser pulses with dielectric materials: insights from numerical modelling," J. Optoelectron. *Adv. M.* 12, pp. 470-473 (2010).

[5] *Femtosecond Laser Micromachining*, R. Osellame, G. Cerullo, and R. Ramponi, Springer Berlin Heidelberg, (2012).

[6] M. Malinauskas, A. Žukauskas, S. Hasegawa, Y. Hayasaki, V. Mizeikis, R. Buividas, and S. Joudkazis "Ultrafast laser processing of materials: from science to industry," *Light: Sci. Appl.* 5, e16133 (2016).

[7] M. Ali, T. Wagner, M. Shakoor, and P. A. Molian, "Review of laser nanomachining," *J. Laser Appl.* 20, pp. 169–184 (2008).

[8] S. Gross and M. J. Withford, "Ultrafast-laser-inscribed 3D integrated photonics: challenges and emerging applications," *Nanoph.* 4, pp. 332-352 (2015).

[9] *Nonlinear Optics*, R. W. Boyd, Academic Press (2007)

[10] V. Nathan, A. H. Guenther, and S. S. Mitra, "Review of multiphoton absorption in crystalline solids," *J. Opt. Soc. Am. B* 2, pp. 294-316 (1985).

[11] L. V. Keldysh, "Ionization in the field of a strong electromagnetic wave," *Sov. Phys. JETP* 20, pp. 1307–1314 (1965).

[12] T. E. Itina and N. Shcheblanov, "Electronic excitation in femtosecond laser interactions with wide-band-gap materials," *Appl. Phys. A* 98, pp. 769–775 (2010).

[13] D. Grojo, M. Gertsvolf, S. Lei, T. Barillot, D. M. Rayner, and P. B. Corkum, "Exciton-seeded multiphoton ionization in bulk SiO_2," *Phys. Rev. B* 81, 212301 (2010).

[14] L. V. Keldysh, "Behavior of non-metallic crystals in strong electric fields," *Sov. Phys. JETP* 6, pp. 763–770 (1958).

[15] Defects in SiO_2 and Related Dielectrics: Science and Technology, G. Pacchioni, L. Skuja, and D. L. Griscom, Springer Netherlands (2000).

[16] B. Poumellec, M. Lancry, A. Chahid-Erraji, and P. G. Kazansky, "Modification thresholds in femtosecond laser processing of pure silica: review of dependencies on laser parameters," *Opt. Mater. Express* 1, pp. 766-782 (2011).

[17] A. Alessi, C. D'Amico, S. Girard, M. Royon, F. Youssef, M. Raine, M. Gaillardin, N. Richard, P. Paillet, R. Stoian, A. Boukenter, and Y. Ouerdane, "Confocal-micro-luminescence characterization of femtosecond laser irradiated silica and borosilicate glasses," *Nuclear Inst. and Methods in Physics Research B* 435, pp. 251–257 (2018).

[18] M. Royon, E. Marin, S. Girard, A. Boukenter, Y. Ouerdane, and R. Stoian, "X-ray preconditioning for enhancing refractive index contrast in femtosecond laser photoinscription of embedded waveguides in pure silica," *Opt. Mater. Express* 9, pp. 65-74 (2019).

[19] V. De Michele, M. Royon, E. Marin, A. Alessi, A. Morana, A. Boukenter, M. Cannas, S. Girard, and Y. Ouerdane, "Near-IR- and UV-femtosecond laser waveguide inscription in silica glasses," *Opt. Mater. Express* 9, pp. 4624-4633 (2019).

[20] L. Vaccaro, M. Cannas, B. Boizot, and A. Parlato, "Radiation induced generation of non-bridging oxygen hole center in silica: Intrinsic and extrinsic processes," *J. Non-Cryst. Solids* 353, pp. 586–589 (2007).

[21] L. Skuja, K. Kajihara, M. Hirano, and H. Hosono, "Visible to vacuum-UV range optical absorption of oxygen dangling bonds in amorphous SiO_2," *Phys. Rev. B* 84, 205206 (2011).

[22] A. N. Trukhin, "Temperature dependence of luminescence decay kinetics of self-trapped excitons, germanium and aluminium centres in crystalline quartz," *Phys. stat. sol. (b)* 142, pp. K83–K88 (1987).

[23] K. Tanimura, C. Itoh, and N. Itoh, "Transient optical absorption and luminescence induced by band-to-band excitation in amorphous SiO_2," *J. Phys. C* 21, pp. 1869–1876 (1988).

[24] W. Joosen, S. Guizard, P. Martin, G. Petite, P. Agostini, A. Dos Santos, G. Grillon, D. Hulin, A. Migus, and A. Antonetti, "Femtosecond multiphoton generation of the self-trapped exciton in α-SiO_2," *Appl. Phys. Lett.* 61, pp. 2260–2262 (1992).

[25] T. Uchino, M. Takahashi, and T. Yoko, "Model of oxygen-deficiency-related defects in SiO_2 glass," *Phys. Rev. B* 62, 2983 (2000).

[26] A. N. Trukhin and K. M. Golant, "Peculiarities of photoluminescence excited by 157 nm wavelength F_2 excimer laser in fused and unfused silicon dioxide," *J. Non-Cryst. Sol.* 355, pp. 1719–1725 (2009).

[27] L. Skuja, "Optically active oxygen-deficiency-related centers in amorphous silicon dioxide," *J. Non-Cryst. Sol.* 239, pp. 16–48 (1998).

[28] N. Fukata, Y. Yamamoto, K. Murakami, M. Hase, and M. Kitajima, "In situ spectroscopic measurement of transmitted light related to defect formation in SiO_2 during femtosecond laser irradiation," *Appl. Phys. Lett.* 83, pp. 3495–3497 (2003).

[29] S. Guizard, P. Martin, G. Petite, P. D'Oliveira, and P. Meynadier, "Time-resolved study of laser-induced colour centres in SiO_2," *J. Phys.: Condens. Matter* 8, pp. 1281–1290 (1996).

[30] A. Zoubir, C. Rivero, R. Grodsky, K. Richardson, M. Richardson, T. Cardinal, and M Couzi, "Laser-induced defects in fused silica by femtosecond IR irradiation," *Phys. Rev. B* 73, 224117 (2006).

[31] R. A. Weeks, R. H. Magruder, and A. Stesmans, "Review of some experiments in the 50 year saga of the E′ center and suggestions for future research," *J. Non-Cryst. Sol.* 354, pp. 208–216 (2008).

[32] F. Mangini, M. Ferraro, M. Zitelli, A. Niang, A. Tonello, V. Couderc, and S. Wabnitz, "Multiphoton-absorption-excited up-conversion luminescence in optical fibers," *Phys. Rev. Applied* 14, 054063 (2020).

[33] F. Messina, L. Vaccaro, and M. Cannas, "Generation and excitation of point defects in silica by synchrotron radiation above the absorption edge," *Phys. Rev.* B 81, (2010).

[34] F. Messina, E. Vella, M. Cannas, and R. Boscaino, "Evidence of Delocalized Excitons in Amorphous Solids," P*hys. Rev. Lett.* 105, (2010).

[35] V. De Michele, E. Marin, A. Boukenter, M. Cannas, S. Girard, and Y. Ouerdane, "Photoluminescence of Point Defects in Silicon Dioxide by Femtosecond Laser Exposure", *Phys. Status Solidi A* 200802 (2021).